Elastic properties, structures and phase transitions in model colloids

2004 J. Phys.: Condens. Matter 16 S4115

(http://iopscience.iop.org/0953-8984/16/38/026)

INSTITUTE OF PHYSICS PUBLISHING JOURNAL OF PHYSICS: CONDENSED MATTER

J. Phys.: Condens. Matter **16** (2004) S4115–S4136 PII: S0953-8984(04)79757-X

Elastic properties, structures and phase transitions in model colloids

P Nielaba[1,4], K Binder[2], D Chaudhuri[3], K Franzrahe[1], P Henseler[1], M Lohrer[1], A Ricci[2], S Sengupta[3] and W Strepp[1]

[1] Physics Department, University of Konstanz, 78457 Konstanz, Germany
[2] Physics Department, University of Mainz, 55099 Mainz, Germany
[3] S N Bose National Centre for Basic Sciences, Block JD, Sector III, Salt Lake, Calcutta 700098, India

E-mail: peter.nielaba@uni-konstanz.de

Received 26 April 2004
Published 10 September 2004
Online at stacks.iop.org/JPhysCM/16/S4115
doi:10.1088/0953-8984/16/38/026

Abstract

The nature of the melting transition for a system of hard discs with translational degrees of freedom in two spatial dimensions has been analysed by a combination of computer simulation methods and a finite size scaling technique. The behaviour of the system is consistent with the predictions of the Kosterlitz–Thouless–Halperin–Nelson–Young (KTHNY) theory.

The structural and elastic properties of binary colloidal mixtures in two and three spatial dimensions are discussed as well as those of colloidal systems with quenched point impurities.

Hard and soft discs in external periodic (light-) fields show rich phase diagrams including freezing and melting transitions when the density of the system is varied. Monte Carlo simulations for detailed finite size scaling analysis of various thermodynamic quantities like the order parameter, its cumulants, etc, have been used in order to map the phase diagram of the system for various values of the density and the amplitude of the external potential. For hard discs we find clear indication of a reentrant liquid phase over a significant region of the parameter space. The simulations therefore show that the system of hard discs behaves in a fashion similar to charge stabilized colloids which are known to undergo an initial freezing, followed by a remelting transition as the amplitude of the imposed modulating field produced by crossed laser beams is steadily increased. Detailed analysis of the simulation data shows several features consistent with a recent dislocation unbinding theory of laser induced melting. The differences and similarities of systems with soft potentials (DLVO, $1/r^{12}$, $1/r^6$) and the relation to experimental data is analysed.

(Some figures in this article are in colour only in the electronic version)

[4] Author to whom any correspondence should be addressed.

1. Introduction

During the last decades, crystallization and melting of colloidal suspensions, both in two and three dimensions (2D and 3D), has been a continuous matter of interest. From the experimental point of view the research mostly focused on the analysis of structure and dynamics of the colloidal systems on different length and time scales through static or dynamic light scattering techniques. On the other hand, in theory the nature of the melting transition in 2D has been controversially discussed at least since the work of Kosterlitz and Thouless (KTHNY-theory). Obviously elastic constants play a crucial role in the solid to liquid phase transition: in 2D the KTHNY theory even claims that the melting process is entirely controlled by the elastic constants. However, both experimental and simulation studies of elastic constants are quite rare. Therefore, the development of tools for the determination of elastic constants in (colloidal) model systems is important.

The simulational approach makes use of a new coarse-graining procedure which has been successfully tested for a hard disc system. In this technique, elastic strains are calculated from the instantaneous configurations of the particles and averaged over sub-blocks of various linear dimensions $L_b \leqslant L$ of a system of total linear dimension L. From these data the correlation function of strain fluctuations in the thermodynamic limit can be extracted and the elastic constants then inferred from well known fluctuation formula.

This method is applied to models of colloidal systems containing quenched point impurities and to colloidal mixtures. Interesting high pressure structures are found for colloidal mixtures in two and three dimensions. Anisotropic situations caused by thin films of thickness D are considered as well, and interesting modifications of the solid structures close to walls are found.

Hard and soft discs in external periodic (light-) fields show rich phase diagrams including freezing and melting transitions when the density of the system is varied. By Monte Carlo simulation methods we have investigated the interesting phase diagrams of such systems for various values of the density and the amplitude of the external potential.

Here we give an overview of the new method for the computation of elastic constants and the application to various systems, on the behaviour of colloids in external light fields, and we report on interesting recent results.

2. Elastic constants from microscopic strain fluctuations

2.1. The method

One is often interested in long length scale and long time scale phenomena in solids (e.g. late stage kinetics of solid state phase transformations; motion of domain walls interfaces; fracture; friction; etc). Such phenomena are usually described by continuum theories. Microscopic simulations [1, 2] of finite systems, on the other hand, like molecular dynamics, lattice Boltzmann or Monte Carlo, deal with microscopic variables like the positions and velocities of constituent particles, and, together with detailed knowledge of interatomic potentials, hope to build up a description of the macro system from a knowledge of these micro variables. How does one recover continuum physics from simulating the dynamics of N particles? This requires a 'coarse-graining' procedure in space (for equilibrium) or both space and time for non-equilibrium continuum theories. Over what coarse graining length and time scale does one recover results consistent with continuum theories? We attempted to answer these questions [3] for the simplest nontrivial case, namely, a crystalline solid, (without any point, line or surface defects [4]) in equilibrium, at a non-zero temperature far away from phase transitions.

Consider a general system described by a scalar order parameter $\phi(\mathbf{r})$ and the free energy functional

$$F[\phi(\mathbf{r})] = k_{\mathrm{B}}T \int \mathrm{d}^d r \left(\tfrac{1}{2} r\phi^2 + \tfrac{1}{2} c \nabla\phi(\mathbf{r})^2\right). \tag{1}$$

This implies a correlation function $G(q)$ in the high temperature phase $T > T_{\mathrm{c}}$ ($\langle\phi\rangle = 0$) of the Ornstein–Zernike form

$$\beta G(q) = \langle \phi_q \phi_{-q} \rangle = \chi^{\infty} \frac{1}{1 + (q\xi)^2} \tag{2}$$

(k_{B} is the Boltzmann constant, T the temperature, and $\beta = 1/k_{\mathrm{B}}T$).

In the computer simulation we determine ϕ averaged within a sub-block of size $L_{\mathrm{b}} \leqslant L$,

$$\overline{\phi} = L_{\mathrm{b}}^{-d} \int^{L_{\mathrm{b}}} \mathrm{d}^d r\, \phi(\mathbf{r}). \tag{3}$$

Then the fluctuations of $\overline{\phi}$ obtained within this block are given by

$$\langle \overline{\phi}^2 \rangle_{L_{\mathrm{b}}} L_{\mathrm{b}}^d = L_{\mathrm{b}}^{-d} \int^{L_{\mathrm{b}}} \mathrm{d}^d r' \, \mathrm{d}^d r \, \langle \phi(r)\phi(r') \rangle \tag{4}$$

$$= \int^{L_{\mathrm{b}}} \mathrm{d}^d r \, \beta G(r) \equiv \chi^{L_{\mathrm{b}}}, \tag{5}$$

where $G(r)$ is the inverse Fourier transform of the correlation function defined in (2).

This concept has been proven to be very useful for Ising-type systems. Here we discuss the generalization of the concept to systems where the important degree of freedom is the strain field, which is of tensor character rather than scalar.

Fluctuations of the instantaneous local Lagrangian strain $\epsilon_{ij}(\mathbf{r}, \mathbf{t})$, determined with respect to a static 'reference' lattice, are used to obtain accurate estimates of the elastic constants of model solids from atomistic computer simulations. The computed strains are systematically coarse-grained by averaging them within subsystems (of size L_{b}) of a system (of total size L) in the canonical ensemble, $\bar{\epsilon}_{ij} = L_{\mathrm{b}}^{-d} \int^{L_{\mathrm{b}}} \mathrm{d}^d r\, \epsilon_{ij}(\mathbf{r})$. Using the finite size scaling ideas outlined below we predict the behaviour of the fluctuations $\langle \bar{\epsilon}_{ij} \bar{\epsilon}_{kl} \rangle$ as a function of L_{b}/L and extract elastic constants of the system *in the thermodynamic limit* at non-zero temperature. Our method is simple to implement, efficient and general enough to be able to handle a wide class of model systems including those with singular potentials without any essential modification.

Imagine a system in the constant NVT (canonical) ensemble at a fixed density $\rho = N/V$ evolving in time t. For any 'snapshot' of this system taken from this ensemble, the local instantaneous displacement field $\mathbf{u}_{\mathbf{R}}(t)$ defined over the set of lattice vectors $\{\mathbf{R}\}$ of a reference lattice (at the same density ρ) is $\mathbf{u}_{\mathbf{R}}(t) = \mathbf{R}(t) - \mathbf{R}$, where $\mathbf{R}(t)$ is the instantaneous position of the particle tagged by the reference lattice point $\mathbf{R}$. Let us concentrate only on perfect crystalline lattices; if topological defects such as dislocations are present the analysis below needs to be modified. The instantaneous Lagrangian strain tensor ϵ_{ij} defined at $\mathbf{R}$ is then given by [4]

$$\epsilon_{ij} = \frac{1}{2} \left(\frac{\partial u_i}{\partial R_j} + \frac{\partial u_j}{\partial R_i} + \frac{\partial u_i}{\partial R_k} \frac{\partial u_k}{\partial R_j} \right). \tag{6}$$

The strains considered here are always small and so we, hereafter, neglect the non-linear terms in the definition given above for simplicity. The derivatives are required at the reference lattice points $\mathbf{R}$ and can be calculated by any suitable finite difference scheme once $\mathbf{u}_{\mathbf{R}}(t)$ is known. We are now in a position to define coarse grained variables $\bar{\epsilon}_{ij}$ which are simply averages of the strain over a sub-block of size L_{b}. The fluctuation of this variable then defines the size dependent compliance matrices $S_{ijkl}^{L_{\mathrm{b}}} = L_{\mathrm{b}}^d \langle \bar{\epsilon}_{ij} \bar{\epsilon}_{kl} \rangle$.

2.2. Two-dimensional systems

Before proceeding further, we introduce a compact Voigt notation (which replaces a pair of indices ij by one α) appropriate for two-dimensional strains—the case considered in this subsection. Using $1 \equiv x$ and $2 \equiv y$, we have

$$ij \quad = \quad 11 \quad 22 \quad 12 \qquad \alpha \quad = \quad 1 \quad 2 \quad 3. \tag{7}$$

The non-zero components of the compliance matrix are

$$S_{11}^{L_b} = L_b^2\langle\bar{\epsilon}_{xx}\bar{\epsilon}_{xx}\rangle = S_{22}^{L_b} \qquad S_{12}^{L_b} = L_b^2\langle\bar{\epsilon}_{xx}\bar{\epsilon}_{yy}\rangle = S_{21}^{L_b} \qquad S_{33}^{L_b} = 4L_b^2\langle\bar{\epsilon}_{xy}\bar{\epsilon}_{xy}\rangle. \tag{8}$$

It is useful to define the following linear combinations:

$$S_{++}^{L_b} = L_b^2\langle\bar{\epsilon}_{+}\bar{\epsilon}_{+}\rangle = 2(S_{11}^{L_b} + S_{12}^{L_b}) \qquad S_{--}^{L_b} = L_b^2\langle\bar{\epsilon}_{-}\bar{\epsilon}_{-}\rangle = 2(S_{11}^{L_b} - S_{12}^{L_b}), \tag{9}$$

where $\bar{\epsilon}_{+} = \bar{\epsilon}_{xx} + \bar{\epsilon}_{yy}$ and $\bar{\epsilon}_{-} = \bar{\epsilon}_{xx} - \bar{\epsilon}_{yy}$. Once the block averaged strains $\bar{\epsilon}_{ij}$ are obtained, it is straightforward to calculate these fluctuations (for each value of L_b).

The block averaged compliance matrices approach the limiting values for large L_b [3],

$$S_{\gamma\gamma}^{L_b} = S_{\gamma\gamma}^{\infty}\left[\Psi_2(xL/\xi) - \left(\Psi_2(L/\xi) - C\left(\frac{a}{L}\right)^2\right)x^2\right] + \mathcal{O}(x^4), \tag{10}$$

where γ takes the values $+$, $-$ or 3 and $x = L_b/L$, and we have suppressed subscripts on the correlation length ξ and the constant C for clarity. $\Psi_2(\alpha)$ is defined as

$$\Psi_2(\alpha) = \frac{2}{\pi}\alpha^2\int_0^1\int_0^1 \mathrm{d}x\,\mathrm{d}y\,K_0\big(\alpha\sqrt{x^2+y^2}\big), \tag{11}$$

where K_0 is a Bessel function. The above equation (10) can now be used to obtain the *system size independent* quantities $S_{\alpha\beta}^{\infty}$, ξ and C.

Once the finite size scaled compliances are obtained the elastic constants, namely the bulk modulus $B = \rho\partial p/\partial\rho$ and the shear modulus μ, are obtained simply using the formulae [5]

$$\beta B = \frac{1}{2S_{++}^{\infty}} \qquad \beta\mu = \frac{1}{2S_{--}^{\infty}} - \beta p \qquad \beta\mu = \frac{1}{2S_{33}^{\infty}} - \beta p, \tag{12}$$

where we assume that the system is under a uniform hydrostatic pressure p.

As an example we present our results for elastic constants of the hard disc system in figure 1. The two expressions for the shear modulus in equation (12) give almost identical results, and this gives us confidence about the internal consistency of our method. We have also compared our results to those of Wojciechowski *et al* [6]. We find that while their values of the pressure and bulk modulus are in good agreement with ours (and with free volume theory) they grossly overestimate the shear modulus. This is probably due to the extremely small size of their systems and/or insufficient averaging. Our results for the sub-block analysis shows that finite size effects are non-trivial for elastic strain fluctuations and they cannot be evaluated by varying the total size of the system from 24 to 90, an interval which is less than half of a decade. One immediate consequence of our results is that the Cauchy relation [6] $\mu = B/2 - p^*$ is seen to be valid up to $\pm 15\%$ over the entire density range we studied, though there is a systematic deviation which changes sign, going from negative for small densities to positive as the density is increased. This is in agreement with the usual situation in a variety of real systems [7] with central potentials and highly symmetric lattices, and in disagreement with [6]. We have also compared our estimates for the elastic constants with the density functional theory (DFT) of Ryzhov and Tareyeva [8]. We find that both the bulk and the shear moduli are grossly overestimated—sometimes by as much as 100%.

By application of such a method to configurations obtained experimentally by video microscopy methods it was possible to analyse precisely experimental results on the elasticity of colloidal systems [9].

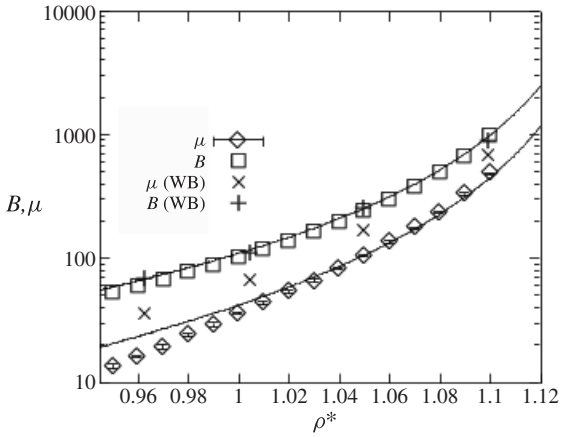

Figure 1. The bulk (B) and shear (μ) moduli in units of $k_B T/\sigma^2$ for the hard disc solid. Our results for B (μ) are given by squares (diamonds). The values for the corresponding quantities from [6] are given by + and $\times$. The curve through the bulk modulus values is the analytical expression obtained from the free volume prediction for the pressure. The curve through our shear modulus values is obtained from the free volume bulk modulus using the Cauchy relation $\mu = B/2 - p$. From Sengupta *et al* [3, 18].

2.3. One-dimensional systems

In order to analyse the finite-size scaling features of our method in more detail, we present here the scaling analysis for a one-dimensional harmonic chain with lattice constant a, for which the scaling form can be computed analytically [10].

The free energy is given by

$$F = \int \mathrm{d}x \, \frac{B}{2}\epsilon^2$$

with strain $\epsilon = \frac{\partial u}{\partial x}$ and bulk modulus B. An arbitrary lattice-phonon has the form

$$s_n = A\cos(qna - \omega t) + C\sin(qna - \omega t).$$

The calculation of the canonical ensemble average $\mathcal{S}^{L_b} = L_b\langle\bar{\epsilon}^2\rangle$ yields the following scaling law ($x = L_b/L$):

$$x\mathcal{S}^{L_b} = K_1 x + K_2 x^2 N + \frac{K_3}{N}, \tag{13}$$

where K_1, K_2 and K_3 are constants and N is the number of particles in the system.

In figure 2 we show that indeed the results for the compliance matrix obtained with our method follow closely the shape of the simple parabola resulting in equation (13).

2.4. Three-dimensional systems

An analysis of the finite size scaling method in three dimensions [11] reveals that quantities in the thermodynamic limit in three dimensions are obtained by fitting data to the form ($x = L_b/L$)

$$\chi^{L_b} = \chi^{\infty}\left[\Psi_3(xL/\xi) - \Psi_3(L/\xi)x^3\right] + \mathcal{O}(x^4), \tag{14}$$

where the function $\Psi_3(\alpha)$ is defined for a three-dimensional system as

$$\Psi_3(\alpha) = 1 - \mathrm{e}^{-\alpha}(\alpha + 1). \tag{15}$$

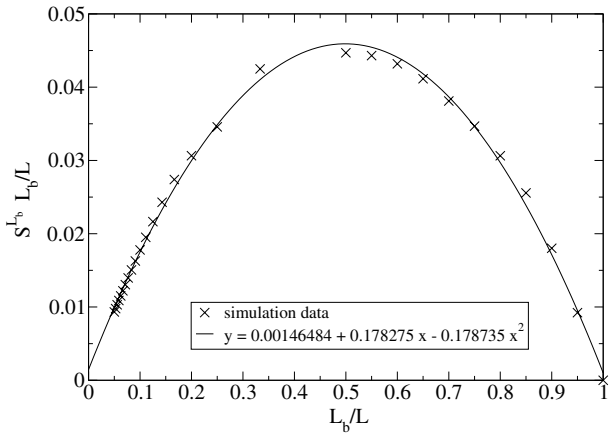

Figure 2. Strain–strain fluctuations or elements of the compliance matrix $\mathcal{S}$ for a one-dimensional periodic harmonic chain as a function of relative sub-block size L_b/L, symbols: simulation data; curve: fit to the scaling function equation (13). The results (symbols) shown are for a system of $N = 500$ particles at $\rho^* = 1.0$, $\beta = 1$, spring constant $= 1$. In a run with 3×10^6 Monte Carlo steps (MCS) 3×10^5 data points have been sampled after an equilibration of 10^6 MCS.

For $L_b \to L$ the block-averaged fluctuation quantity approaches zero, $\chi^{L_b} \to 0$. In the case when the correlation length ξ is small compared to the system size L, then $\Psi_3(\alpha) \to 1$, and equation (14) goes over to the simple form

$$\chi^{L_b} \cdot x = \chi^{\infty}[x - x^4]. \tag{16}$$

The elastic free energy of a cubic crystal is

$$F_{\text{elast}} = \tfrac{1}{2} \int \mathrm{d}^3 r \{C_{11}(\varepsilon_{xx}^2 + \varepsilon_{yy}^2 + \varepsilon_{zz}^2) + 2C_{12}(\varepsilon_{xx}\varepsilon_{yy} + \varepsilon_{xx}\varepsilon_{zz} + \varepsilon_{yy}\varepsilon_{zz}) + 4C_{44}(\varepsilon_{xy}^2 + \varepsilon_{xz}^2 + \varepsilon_{yz}^2)\} \tag{17}$$

$$= \tfrac{1}{2} \int \mathrm{d}^3 r \big\{A(\varepsilon_{xx} + \varepsilon_{yy} + \varepsilon_{zz})^2 + B\left[(\varepsilon_{xx} - \varepsilon_{yy})^2 + (\varepsilon_{xx} - \varepsilon_{zz})^2 + (\varepsilon_{yy} - \varepsilon_{zz})^2\right] + 4C_{44}(\varepsilon_{xy}^2 + \varepsilon_{xz}^2 + \varepsilon_{yz}^2)\big\}, \tag{18}$$

where

$$C_{11} = A + 2B \tag{19}$$

$$C_{12} = A - B. \tag{20}$$

In three dimensions we use the following Voigt-notation ($1 = x$, $2 = y$, $3 = z$):

ij	=	11	22	33	23	13	12
α	=	1	2	3	4	5	6.

The non-zero components of the compliance matrix are

$$S_{++}^{L_b} = L_b^3 \langle(\bar{\epsilon}_{xx} + \bar{\epsilon}_{yy} + \bar{\epsilon}_{zz})^2\rangle$$

$$S_{12}^{L_b} = L_b^3 \langle(\bar{\epsilon}_{xx} - \bar{\epsilon}_{yy})^2\rangle = S_{13}^{L_b} = S_{23}^{L_b}$$

$$S_{44}^{L_b} = 4L_b^3 \langle\bar{\epsilon}_{xy}\bar{\epsilon}_{xy}\rangle = S_{55}^{L_b} = S_{66}^{L_b}.$$

We are interested in the elastic properties far away from phase transition points; under these conditions we use equation (14) up to third order in x:

$$S_{\gamma\gamma}^{L_b} \cdot x = S_{\gamma\gamma}^{\infty}\left[x\Psi_3(xL/\xi) - x^4\left(\Psi_3(L/\xi) - C'(a/L)^3\right)\right]. \tag{21}$$

Using the equipartition theorem, the elastic constants finally can be obtained from

$$\beta A = \frac{1}{2S_{++}^{\infty}} \qquad \beta B = \frac{1}{2S_{12}^{\infty}} = \frac{1}{2S_{13}^{\infty}} = \frac{1}{2S_{23}^{\infty}} \qquad \beta C_{44} = \frac{1}{2S_{44}^{\infty}} = \frac{1}{2S_{55}^{\infty}} = \frac{1}{2S_{66}^{\infty}}$$

and equations (19), (20).

Returning to the $d = 2$ case, we briefly review the successful applications of equations (7)–(12) to a monodisperse system, before we show first applications to other systems.

3. Melting of hard discs in two dimensions

One of the first continuous systems to be studied by computer simulations [12] is the system of hard discs of diameter σ interacting with the two-body potential,

$$U(r) = \begin{cases} \infty & r \leqslant \sigma \\ 0 & r > \sigma, \end{cases} \tag{22}$$

where σ (taken to be 1 in the rest of the paper), the hard disc diameter, sets the length scale for the system and the energy scale is set by $k_{\mathrm{B}}T = 1$. Despite its simplicity, this system was shown to undergo a phase transition from solid to liquid as the density ρ was decreased. The nature of this phase transition, however, is still being debated. Early simulations [12] always found strong first order transitions. As computational power increased the observed strength of the first order transition progressively decreased! Using sophisticated techniques, Lee and Strandburg [13] and Zollweg and Chester [14] found evidence for, at best, a weak first order transition. A first order transition has also been predicted by theoretical approaches based on density functional theory [15, 8]. On the other hand, recent simulations of hard discs [16] find evidence for a KTHNY transition [17] from liquid to a hexatic phase, with orientational but no translational order, at $\rho = 0.899$. Nothing could be ascertained, however, about the expected transition from the hexatic phase to the crystalline solid at higher densities because the computations became prohibitively expensive. The solid to hexatic melting transition was estimated to occur at a density $\rho_{\mathrm{c}} \geqslant 0.91$. *A priori*, it is difficult to assess why various simulations give contradicting results concerning the order of the transition. In [18] we took an approach, complementary to Jaster's [16], and investigated the melting transition of the solid phase. We showed that the hard disc solid is unstable to perturbations which attempt to produce free dislocations leading to a solid $\rightarrow$ hexatic transition in accordance with KTHNY theory [17] and recent experiments in colloidal systems [19]. Though this has been attempted in the past [6, 20], numerical difficulties, especially with regard to equilibration of defect degrees of freedom, makes this task highly challenging. The elastic Hamiltonian for hard discs is given by $F = -p\epsilon_+^2 + (B/2)\epsilon_+^2 + (\mu + p)(\epsilon_-^2/2 + 2\epsilon_{xy}^2)$, where B is the bulk modulus. The quantity $\mu_{\mathrm{eff}} = \mu + p$ is the 'effective' shear modulus (the slope of the shear stress versus shear strain curve) and p is the pressure.

The KTHNY theory [17] is presented usually for a 2D triangular solid under *zero external stress*. It is shown that the dimensionless Young's modulus of a 2D solid, $K = (8/\sqrt{3}\rho)(\mu/\{1 + \mu/(\lambda + \mu)\})$, where μ and λ are the Lamé constants, depends on the fugacity of dislocation pairs, $y = \exp(-E_{\mathrm{c}})$, where E_{c} is the core energy of the dislocation, and the 'coarse-graining' length scale l. This dependence is expressed in the form of the following coupled recursion relations for the renormalization of K and y:

$$\begin{aligned} \frac{\partial K^{-1}}{\partial l} &= 3\pi y^2 \mathrm{e}^{\frac{K}{8\pi}} \left[\frac{1}{2} I_0\left(\frac{K}{8\pi}\right) - \frac{1}{4} I_1\left(\frac{K}{8\pi}\right) \right], \\ \frac{\partial y}{\partial l} &= \left(2 - \frac{K}{8\pi}\right) y + 2\pi y^2 \mathrm{e}^{\frac{K}{16\pi}} I_0\left(\frac{K}{8\pi}\right), \end{aligned} \tag{23}$$

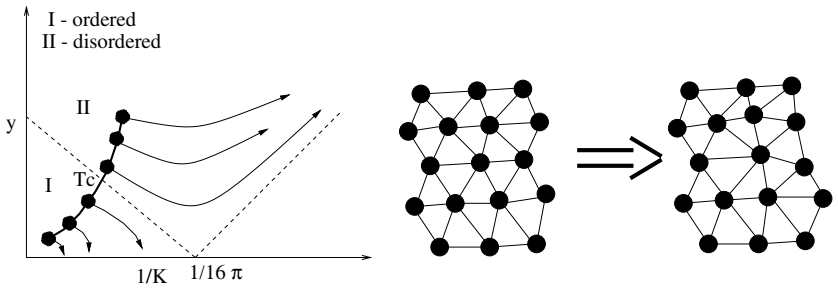

Figure 3. Left: schematic flows of the coupling constant K and the defect fugacity y under the action of the KTHNY recursion relations. The dashed line is the separatrix whose intersection with the line of initial state (solid curve connecting filled circles, $y(T, l = 0)$, $K^{-1}(T, l = 0)$) determines the transition point T_c. Right: typical move which attempts to change the coordination number and therefore the local connectivity around the central particle. Such moves were rejected in our simulation.

where I_0 and I_1 are Bessel functions. The thermodynamic value is recovered by taking the limit $l \to \infty$.

We see in figure 3 that the trajectories in the y–K plane can be put in two classes, namely those for which $y \to 0$ as $l \to \infty$ (ordered phase) and those for which $y \to \infty$ as $l \to \infty$ (disordered phase). These two classes of flows are separated by a line called the separatrix. The transition temperature T_c (or ρ_c) is given by the intersection of the separatrix with the line of initial conditions $K(\rho, T)$ and $y = \exp(-E_c(K))$, where $E_c \sim cK/16\pi$. The disordered phase is a phase where free dislocations proliferate. Proliferation of dislocations, however, *does not* produce a liquid, but rather a liquid crystalline phase called a 'hexatic' with quasi-long ranged (QLR) orientational order but short ranged positional order. A *second* KTHNY transition destroys QLR orientational order and takes the hexatic to the liquid phase by the proliferation of 'disclinations' (scalar charges). Apart from T_c there are several universal predictions from KTHNY theory: for example, the order parameter correlation length and susceptibility have essential singularities ($\sim e^{bt^{-\nu}}$, $t \equiv T/T_c - 1$) near T_c. All these predictions can, in principle, be checked in simulations [16].

One way to circumvent the problem of large finite size effects and slow relaxation due to diverging correlation lengths is to simulate a system which is constrained to remain defect (dislocation) free and, as it turns out, without a phase transition. Surprisingly, using this data it is possible to predict the expected equilibrium behaviour of the unconstrained system. The simulation [18] is always started from a perfect triangular lattice which fits into our box, the size of the box determining the density. Once a regular Monte Carlo (MC) move is about to be accepted, we perform a *local* Delaunay triangulation involving the moved disc and its nearest and next nearest neighbours. We compare the connectivity of this Delaunay triangulation with that of the reference lattice (a copy of the initial state) around the same particle. If any old bond is broken and a new bond formed (figure 3) we reject the move since one can show that this is equivalent to a dislocation–antidislocation pair separated by one lattice constant involving dislocations of the smallest Burger's vector.

Microscopic strains $\epsilon_{ij}(\mathbf{R})$ can be calculated now for every reference lattice point $\mathbf{R}$. Next, we coarse grain (average) the microscopic strains within a sub-box of size L_b and calculate the (L_b dependent) quantities [3]

$$S_{++}^{L_b} = L_b^2 \langle \bar{\epsilon}_+ \bar{\epsilon}_+ \rangle, \qquad S_{--}^{L_b} = L_b^2 \langle \bar{\epsilon}_- \bar{\epsilon}_- \rangle, \qquad S_{33}^{L_b} = 4L_b^2 \langle \bar{\epsilon}_{xy} \bar{\epsilon}_{xy} \rangle. \tag{24}$$

The elastic constants in the thermodynamic limit are obtained from the set $B = 1/(2S^{\infty}_{++})$ and $\mu_{\rm eff} = 1/(2S^{\infty}_{--}) = 1/(2S^{\infty}_{33})$. We obtain highly accurate values of the unrenormalized coupling constant K and the defect fugacity y which can be used as inputs to the KTHNY recursion relations. Numerical solution of these recursion relations then yields the renormalized coupling $K_{\rm R}$ and hence the density and pressure of the solid to hexatic melting transition.

We can draw a few very precise conclusions from our results. Firstly, a solid without dislocations is stable against fluctuations of the amplitude of the solid order parameter and against long wavelength phonons. So any melting transition mediated by phonon or amplitude fluctuations is ruled out in our system. Secondly, the core energy $E_{\rm c} > 2.7$ at the transition, so KTHNY perturbation theory is valid though numerical values of nonuniversal quantities may depend on the order of the perturbation analysis. Thirdly, solution of the recursion relations shows that a KTHNY transition at $p_{\rm c} = 9.39$ *preempts* the first order transition at $p_1 = 9.2$. Since these transitions, as well as the hexatic–liquid KTHNY transition, lie so close to each other, the effect of (as yet unknown) higher order corrections to the recursion relations may need to be examined in the future. Due to this caveat, our conclusion that a hexatic phase exists over some region of density exceeding $\rho = 0.899$ still must be taken as preliminary [21]. Also, in actual simulations, cross-over effects near the bicritical point, where two critical lines corresponding to the liquid–hexatic and hexatic–solid transitions meet a first order liquid–solid line, may complicate the analysis of the data, which may, in part, explain the confusion which persists in the literature on this subject.

4. Solid structures of soft disc systems near walls

In this section we present some computational results [22] for a soft discs triangular crystal in a confined geometry. We perform standard NVT Monte Carlo simulations. First we investigate how the crystal rearranges itself in the presence of the wall. We compute the change in the distance and in the orientation between crystal planes with respect to the bulk case. During the simulation the system is constrained to remain free of defects.

As interaction potential we chose a truncated repulsive Lennard-Jones interaction:

$$U(r) = \begin{cases} \epsilon\left(\dfrac{\sigma}{r}\right)^{12} & r < r_{\rm c}, \\ 0 & \text{otherwise}, \end{cases} \tag{25}$$

with a cutoff-distance $r_{\rm c} = 2.5\sigma$. The density is $\rho^* = \rho\sigma^2 = 1.05$ and the temperature is $T^* = k_{\rm B}T/\epsilon = 1$.

We want to study the effect of confinement on the crystal. The confinement is modelled by two perfectly repulsive smooth walls at a distance $D/\sigma = D^*$. The wall–particle interaction potential is either modelled by integration over the repulsive part of the Lennard-Jones interaction,

$$U_{\rm wall}(x) = \epsilon_{\rm wall}\left(\frac{\sigma}{|x - x_{\rm wall}|}\right)^{10}, \tag{26}$$

or simply by hard walls,

$$U_{\rm wall}(x) = \begin{cases} 0 & 0 < x < D^*, \\ \infty & \text{elsewhere}. \end{cases} \tag{27}$$

A cartoon of the system geometry is given in figure 4.

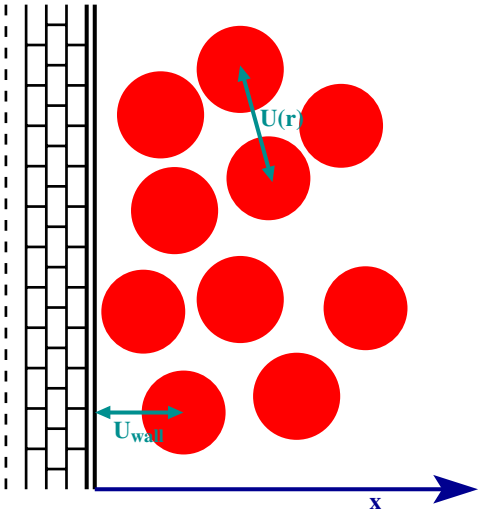

Figure 4. Cartoon of the system geometry.

We simulate with the standard metropolis Monte Carlo algorithm two kinds of systems.

- One of 780 particles which corresponds to 30×26 unit cells of triangular lattice in a nearly square box; the density is $\rho^* = \rho\sigma^2 = 1.05$ and the temperature $T^* = k_B T/\epsilon = 1$. The lattice spacing is $a = \sqrt{\frac{2}{\sqrt{3}\rho}} \approx 1.049$ so the distance between the walls here is $D^* = D\sigma = 30\frac{\sqrt{3}}{2}a \approx 27.245$.
- One of 1200 particles in a box with tilted sides which form an angle of 60°. Here we want to consider a thin film-like case and at the same time we try to simulate better the triangular geometry of the lattice. We consider 60×20 unit cells. The density and the temperature have the same values as in the previous case and so here the distance between the walls is (again in unit of σ) $D^* = 20\frac{\sqrt{3}}{2}a \approx 18.163$.

Regarding the bulk behaviour, at the chosen density and temperature, the soft discs are in the crystal phase [23] but when we introduce walls with a sufficiently small ϵ_{wall} or in case of hard walls, there is no crystal any more after the equilibration as we see in the two snapshots of figure 5.

In order to avoid this problem, and to evaluate properly the local strain field, our simulations are constrained to stay dislocation free as in [18].

We see that, due to the wall, the first lattice planes in the x direction (parallel to the wall) change their spacing in comparison to the bulk case quite significantly; the crystal now is 'squeezed' or 'lengthened' in the x-direction. For the effect of the wall potential, see figure 6.

We further analysed the variation of the angle α between lattice planes; see figure 7. α is now is slightly different from 60°, the value for the undeformed lattice; see figure 7.

5. Colloidal mixtures

We also have considered colloidal mixtures with different diameters in two and three dimensions and the composition dependence of their phase behaviour and the elastic properties. *A priori* it is not obvious if such systems are softer or harder compared to the corresponding monodisperse systems, and a systematic study is required in order to design materials with well defined elastic properties at a later stage. Besides this, already in two spatial dimensions

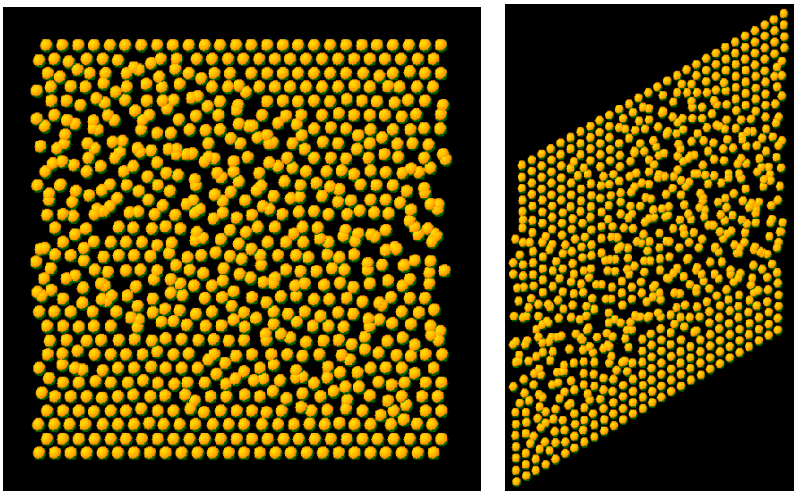

Figure 5. Typical configurations of the system. The walls here are parallel to the short side (left picture) and the tilted side (right picture).

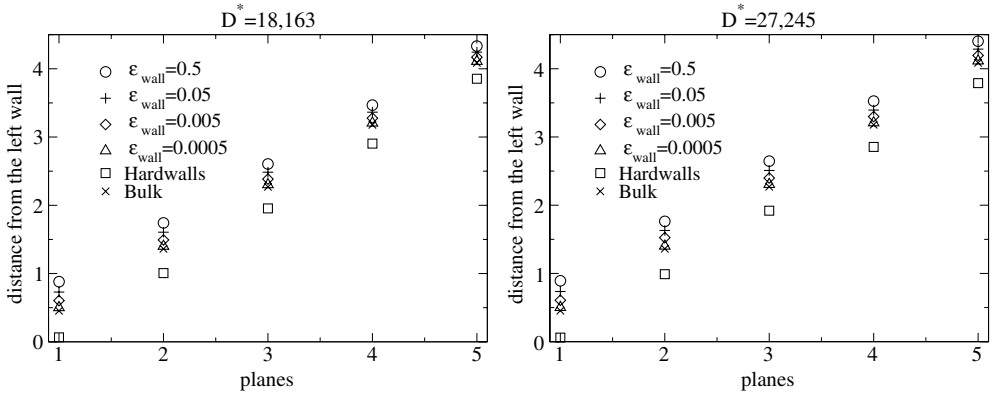

Figure 6. Change in distance between the crystal planes parallel to the wall direction for two wall-distances.

interesting structures have been found which significantly deviate from the traditional triangular lattice for certain diameter ratios.

5.1. Mono-disperse hard sphere system with point-like impurities

In order to analyse the effect of point impurities on the elastic properties of a triangular system of hard discs, we applied our method to the case of quenched impurities with various concentrations [10]. A typical configuration with $N = 3072$ particles and $n = 124$ impurities is shown in figure 8. In a typical run with 6.5×10^6 MCS, 550 000 data points have been sampled after an initial equilibration of 10^6 MCS. A quenched average was obtained by averaging over 100 runs with random placements of the impurities fixed at their initial place. The resulting strain–strain fluctuations for systems with 4% impurities are shown in figure 8. The simulation box has a side length ratio $L_y/L_x = 2/\sqrt{3}$. The elastic constants for various concentrations of point-like impurities can now be obtained by our method, and they are shown in figure 9.

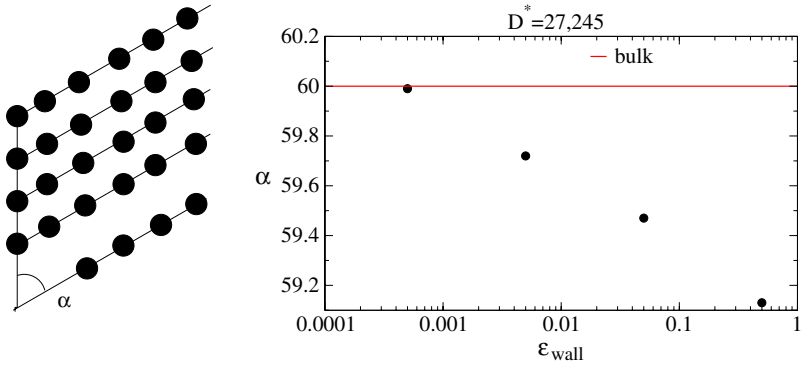

Figure 7. Angle α between lattice planes. Left side: schematic picture. Right side: numerical values according to our simulations; the value of α for hard walls is $\alpha_{\text{hard walls}} = 60.68$.

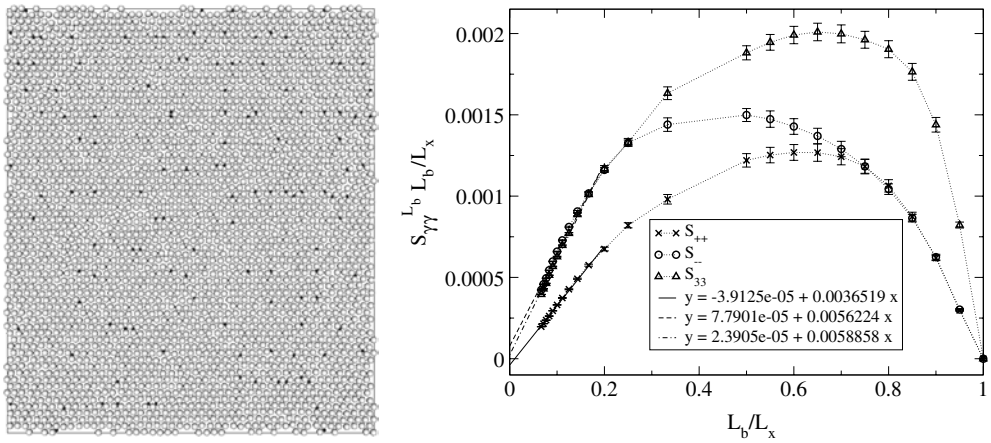

Figure 8. Left: a typical configuration with a random initial placement of $n = 124$ point-like impurities ($N = 3072$, $\varrho^* = 1.0$). Right: quenched average of the strain–strain fluctuations (averages and error bars from 100 runs with random initial placements of 124 point impurities).

We note substantial hardening of the material; already at an impurity concentration of 4% the shear modulus has nearly increased by 100%. The difference in the side lengths L_x and L_y results in a difference between the values for the shear modulus as calculated from S_{--} or S_{33}.

5.2. Binary colloidal mixtures in two dimensions

In order to be able to use our method, the *reference state* **R** must be known. For binary mixtures of hard spheres with different diameters d_A and d_B, thermodynamically stable *reference states* **R** thus must be determined. For this purpose simulations in the NpT ensemble have been done [10]. In these simulations additional *volume-moves* vary the geometry of the system's volume, so that a condensation to a lattice is not inhibited by the geometry of the system's volume.

In figures 10 and 11 we show high pressure phases for binary mixtures of equal concentration $x_A = N_A/N = x_B = N_B/N = 1/2$ and diameter ratios $d_B/d_A = 0.414$ and $d_B/d_A = 0.637$.

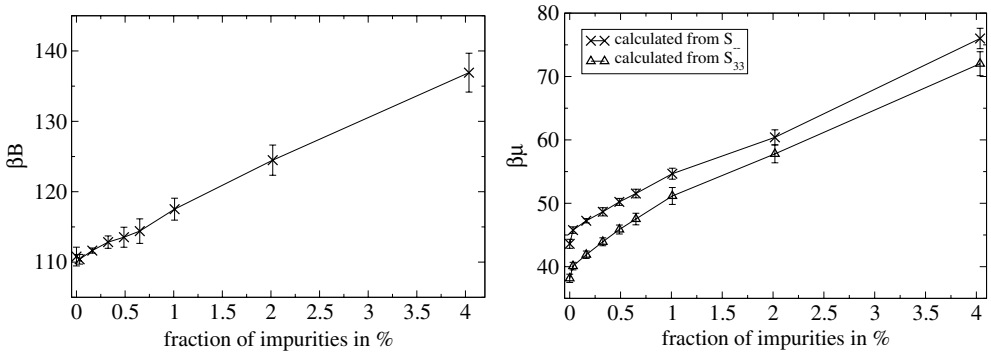

Figure 9. Bulk- (left-hand side) and shear- (right-hand side) modulus of a triangular lattice as a function of impurity concentration (point impurities, quenched average). The error bars are obtained from slope errors in figure 8.

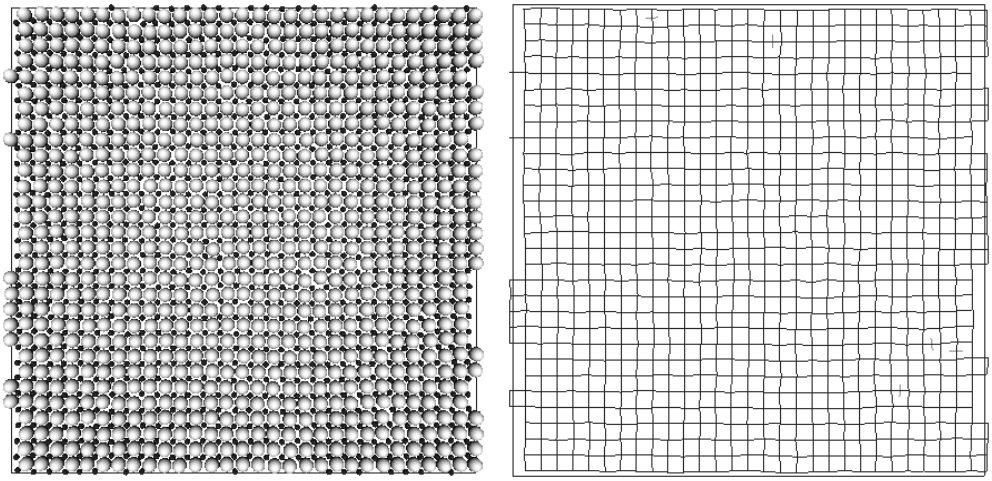

Figure 10. High pressure structures for $p^* = 36$, $N_A + N_B = 1800$, $x_A = x_B = 1/2$, $\frac{d_B}{d_A} = 0.414$. Left: configurations; right: lines connecting nearest neighbours of the same type within $1.3\sigma_A$ or $1.3\sigma_B$, respectively.

For a diameter ratio of 0.414, a square lattice structure is stable. In this case the free energy in terms of elastic constants is

$$F = \int \mathrm{d}^2 r \, \frac{B}{2}\epsilon_+^2 + \frac{\mu_{\mathrm{eff}}}{2}\epsilon_-^2 + 4\frac{\mu'_{\mathrm{eff}}}{2}\epsilon_{xy}^2, \tag{28}$$

where $\mu_{\mathrm{eff}} \neq \mu'_{\mathrm{eff}}$. The strain–strain fluctuations for a system with $N = 3042$ particles at a density $\rho^* = 1.76$ and the resulting elastic constants as functions of the density are shown in figure 12.

5.3. Three-dimensional systems

For various diameter ratios of the hard spheres interesting solid structures appear at high pressure. Example configurations from an NpT simulation of an A–B hard sphere mixture with $N = 1620$ particles, diameter ratio 0.5272 and concentration $x_A = N_A/N = 0.5$ are shown at high and low pressure in figure 13.

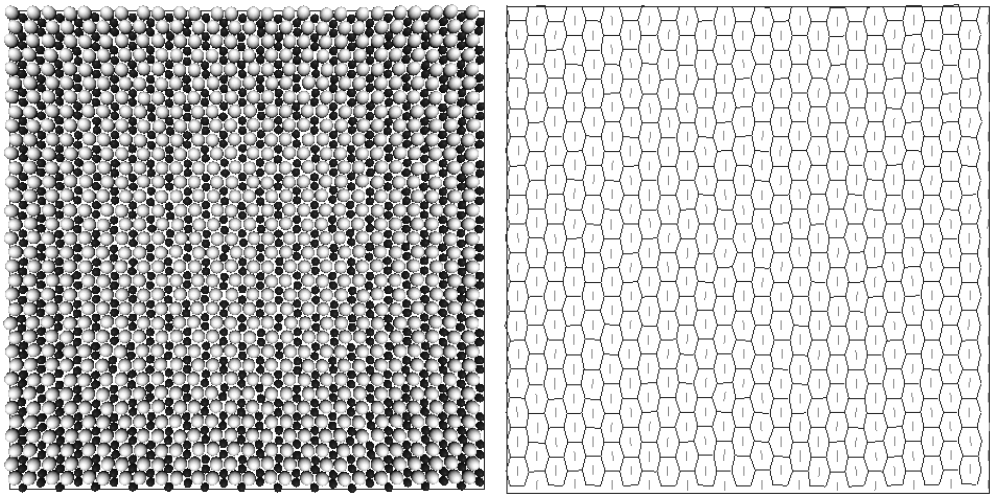

Figure 11. High pressure structures for $p^* = 36$, $N_A + N_B = 1768$, $x_A = x_B = 1/2$, $\frac{d_B}{d_A} = 0.637$. Left: configurations; right: lines connecting nearest neighbours of the same type within $1.3\sigma_A$ or $1.3\sigma_B$, respectively.

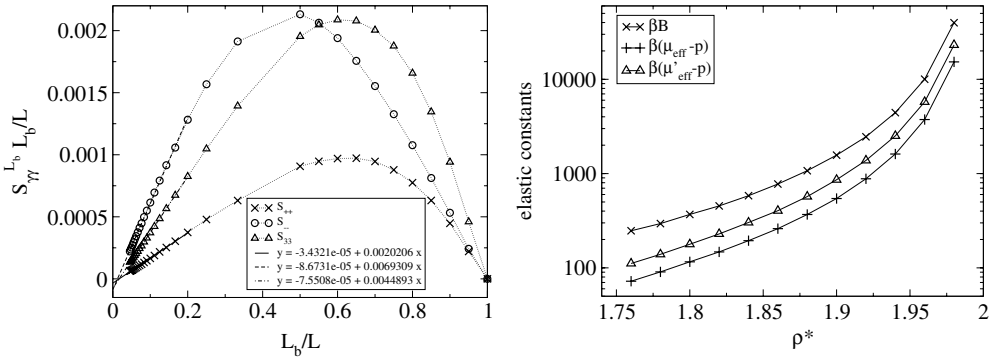

Figure 12. Left: strain–strain fluctuations for $\rho^* = 1.76$; right: elastic constants as functions of density. ($N_A + N_B = 3042$, $x_A = x_B = 1/2$, $d_B/d_A = 0.414$, single runs with an equilibration of 10^6 MCS and an average over 550 000 data points from a simulation with 6.5×10^6 MCS.)

6. Phase transitions of model colloids in external periodic light fields

6.1. Model and method

The liquid–solid transition in two-dimensional systems of particles under the influence of external modulating potentials has recently attracted a fair amount of attention from experiments [24–29, 19], density functional theory [30, 31], dislocation unbinding calculations [32, 17] and computer simulations [33–36]. This is partly due to the fact that well controlled, clean experiments can be performed using colloidal particles [37] confined between glass plates, producing essentially a two-dimensional system. These systems are subjected to a spatially periodic electromagnetic field generated by two interfering crossed laser beams. This field acts on the particles like a commensurate, one dimensional, modulating potential. One of the more surprising results of these studies is the fact that there exist regions

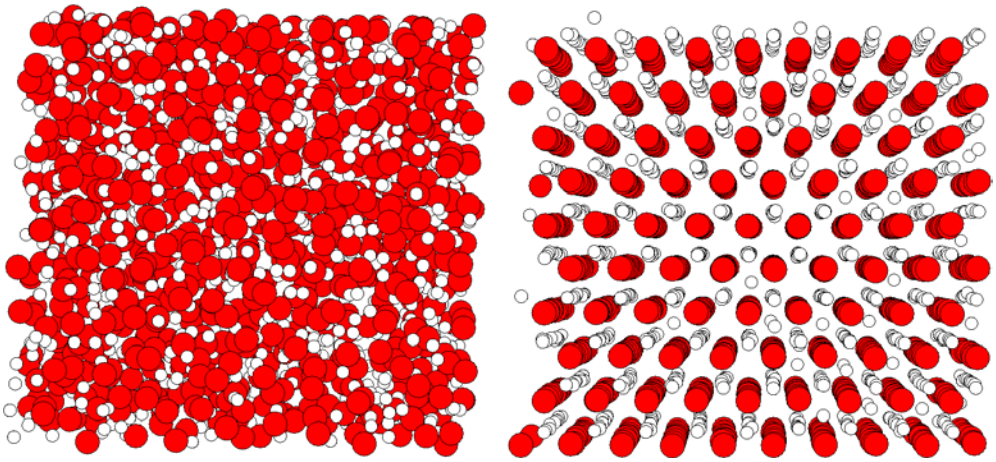

Figure 13. Configurations of an A–B hard sphere mixture ($N = 1620$, $x_A = 0.5$, $d_B/d_A = 0.5272$). Left: disordered configuration at $p^* = 40$; right: slightly distorted configuration at $p^* = 70$. The starting configuration was a perfect ordered AB_2 structure. For clarity reasons the particles are drawn with half of their diameters.

in the phase diagram over which one observes reentrant [27–29] freezing/melting behaviour. As a function of the laser field intensity, the system first freezes from a modulated liquid to a two-dimensional triangular solid. A further increase of the intensity confines the particles strongly within the troughs of the external potential, suppressing fluctuations perpendicular to the troughs, which leads to an uncoupling of neighbouring troughs and to remelting.

Based on these considerations we therefore expect an influence of the range of the particle potential on the width of the freezing and/or reentrance region. In particular, since the fluctuations of the particles perpendicular to the troughs (see the argument above) become less important for longer ranged potentials, we expect the reentrance region to be smaller (or even vanishing) for long ranged potentials.

To clarify the situation, a comparative study [38] of the effect of the range of the interaction potentials on the reentrance region by computer simulations for different types of particle potentials [39–42] has been done, with particular focus on the dependence of the width of the freezing/reentrance region on the particle potential. In addition, experimental results on colloidal particles [29] are compared with our data.

6.1.1. The model. We study a system of N particles in a two-dimensional rectangular box of size $S_x \times S_y$ ($S_x/S_y = \sqrt{3}/2$) and periodic boundary conditions. The particles interact by a pair potential $\phi(r_{ij})$ [37], where r_{ij} is the distance between particle i and j.

We use the following potentials:

- hard discs with diameter σ [39]:

$$\phi(r_{ij}) = \begin{cases} \infty & r_{ij} \leqslant \sigma \\ 0 & r_{ij} > \sigma. \end{cases} \tag{29}$$

  Here we use a reduced density: $\rho^* = \rho\sigma^2$.
- DLVO (Derjaguin, Landau, Vervey and Overbeek) potential [40]:

$$\phi(r_{ij}) = \frac{(Z^*e)^2}{4\pi\epsilon_0\epsilon_r}\left(\frac{\exp(\kappa R)}{1+\kappa R}\right)^2 \frac{\exp(-\kappa r_{ij})}{r_{ij}}, \tag{30}$$

where R is the radius of the particles, $\kappa = \sqrt{\frac{e^2}{\epsilon_0 \epsilon_r k_B T} \sum_i n_i z_i^2}$ the inverse Debye screening length, Z^* the effective surface charge, and ϵ_r the dielectric constant of water. We use $\epsilon_r = 78$, $2R = 1.07\ \mu$m and $Z^* = 7800$. The temperature is chosen as in experimental setups, $T = 293.15$ K (i.e., 20 °C), and the particle density such that the particle spacing in an ideal lattice is $a_s = 2.525\,78\ \mu$m. The different values for the reduced inverse Debye screening length κa_s, which is the dominant parameter here, are obtained by varying κ as required. In addition, we use a cut-off radius r_c: $\phi(r > r_c) = 0$, where r_c obeys the condition $\phi(r_c) = 0.001\ k_B T$.

- algebraic potentials [41, 42]:

$$\phi(r_{ij}) = k_B T / r^n, \tag{31}$$

where we examine $n = 12$ and 6. We chose $r_c = 2$ for $n = 12$, and $r_c = \sqrt{10}$ for $n = 6$.

The forces of the laser field on a particle with coordinates (x, y) is modelled as follows:

$$V(x, y) = V_0\ \sin(2\pi\ x/d_0). \tag{32}$$

The constant d_0 in equation (32) is chosen such that, for a density $\rho = N/(S_x S_y)$, the modulation is commensurate to a triangular lattice of particles with nearest neighbour distance a_s: $d_0 = a_s\sqrt{3}/2$.

The main parameters which define our systems are ρ^* or ρ (or κa_s for the DLVO potential) and the reduced potential strength $V_0/k_B T = V_0^*$.

6.1.2. Observables. In order to obtain thermodynamic quantities for a range of system sizes, we use subsystems of size $L_x \times L_y$, where $L_y = L a_s$ and $L_x = L_y\sqrt{3}/2 = L d_0$.

In the presence of the external potential, we use the positional order parameter ψ_{G_1} to detect the phase transition between modulated liquid (at low density) and crystal (at high density):

$$\psi_{G_1} = \left| \frac{1}{N} \sum_{j=1}^{N} \exp(\mathrm{i}\vec{G}_1 \cdot \vec{r}_j) \right|, \tag{33}$$

where $\vec{r}_j$ is the position vector of the jth particle. $\vec{G}_1$ is one of the six smallest reciprocal lattice vectors of the two-dimensional triangular lattice, pointing in a direction at an angle of $\pi/3$ to the x-axis.

In zero external field the crystal can rotate easily, and we therefore use an orientation-corrected version of ψ_{G_1}, which we denote by $\tilde{\psi}_{G_1}$. The orientation of the crystal can be extracted from the phase information of the orientational order parameter ψ_6. For a particle j located at $\vec{r}_j$ we define the local orientational order:

$$\psi_{6,j} = \frac{1}{N_b} \sum_{l=1}^{N_b} \mathrm{e}^{\mathrm{i}6\theta_{lj}},$$

where N_b is the number of nearest neighbours, and θ_{lj} the angle between the axis $\vec{r}_l - \vec{r}_j$ and an arbitrary reference axis. For the total system we set

$$\psi_6 = \left| \frac{1}{N} \sum_{j=1}^{N} \psi_{6,j} \right|.$$

Properties of these order parameters are described in [40].

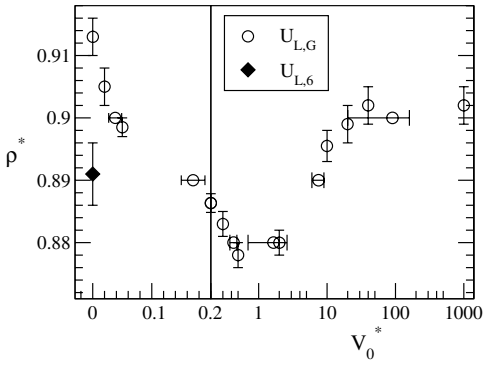

Figure 14. Phase diagram of hard discs ($N = 1024$) [39]. At $V_0^* = 0.2$ a change from a linear to a logarithmic scale on the x-axis is indicated by a vertical line.

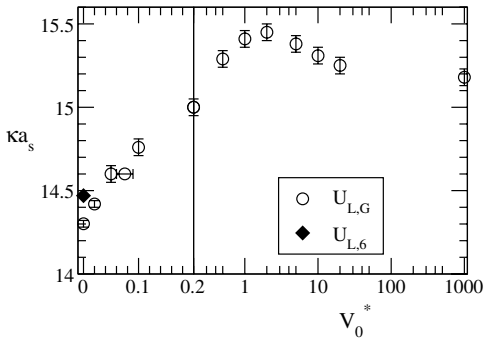

Figure 15. Phase diagram in the case of the DLVO interaction potential ($N = 1024$) [40]. At $V_0^* = 0.2$ a change from a linear to a logarithmic scale on the x-axis is indicated by a vertical line.

Based on these order parameters, we have determined phase transition points by the cumulant intersection method. The fourth order cumulant U_L of the order parameter distribution is given by [43]

$$U_L(V_0^*, \rho^*|\rho|\kappa a_s) = 1 - \frac{\langle \psi_x^4 \rangle_L}{3\langle \psi_x^2 \rangle_L^2}, \tag{34}$$

where ψ_x refers to one of the order parameters described above. In order to distinguish between the cumulants of ψ_6 and ψ_{G_1}, we denote them with $U_{L,6}$ and $U_{L,G}$, respectively. In the liquid (short ranged order) $U_L \to 1/3$, and in the solid (long range order) $U_L \to 2/3$ for $L \to \infty$. In the case of a continuous transition close to the transition point the cumulant is only a function of the ratio of the system size $\approx La_s$ and the correlation length ξ: $U_L(La_s/\xi)$. Since ξ diverges at the critical point the cumulants for different system sizes intersect in one point: $U_{L_1}(0) = U_{L_2}(0) = U^*$. U^* is a non-trivial value, i.e., $U^* \neq 1/3$ and $2/3$. Even for first order transitions these cumulants intersect [44], though the value U^* of U_L at the intersection is not universal any more. The intersection point can, therefore, be taken as the phase boundary regardless of the order of the transition. In the case of a KTHNY transition we expect a merging of the cumulants at the onset of the ordered phase, rather than an intersection point.

In all scenarios the cumulant intersection- or merging points should reliably detect the phase transition. Therefore, in order to map the phase diagram, we systematically vary the system parameters V_0^* and ρ^* or ρ (or κa_s) and identify the cumulant intersection- or merging points with the phase boundary.

6.1.3. Numerical details. Monte Carlo (MC) simulations [45, 1, 2] are done in the NVT ensemble; the total system size is $N = 1024$ or 400. A typical simulation run with 10^7 Monte Carlo steps (MCS) per particle (including 3×10^6 MCS for relaxation) took about 50 CPU hours on a PII/500 MHz PC.

6.2. Results and discussion

6.2.1. Phase diagrams. First we present the phase diagrams for systems with various interaction potentials: hard discs in figure 14 [39], DLVO in figure 15 [40], $1/r^{12}$ in

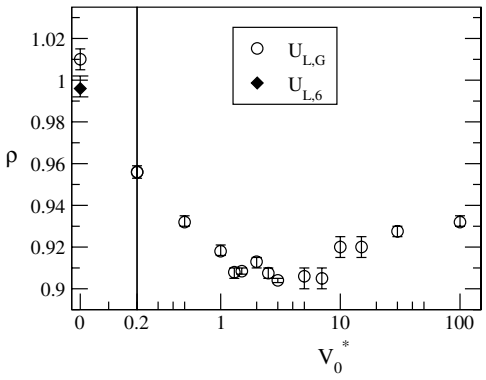

Figure 16. Phase diagram in the case of the $1/r^{12}$ potential ($N = 1024$ particles, except $N = 400$ at $V_0^* = 2.5, 5, 7$) [41, 42]. At $V_0^* = 0.2$ a change from a linear to a logarithmic scale on the x-axis is indicated by a vertical line.

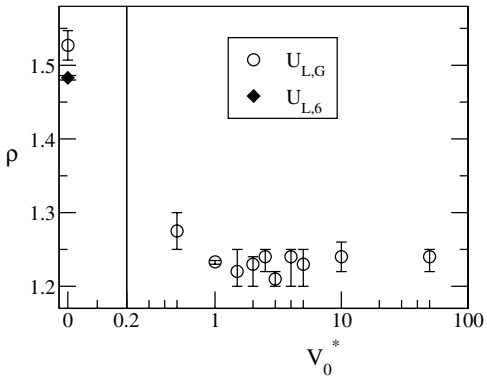

Figure 17. Phase diagram in the case of the $1/r^6$ potential ($N = 400$) [38]. At $V_0^* = 0.2$ a change from a linear to a logarithmic scale on the x-axis is indicated by a vertical line.

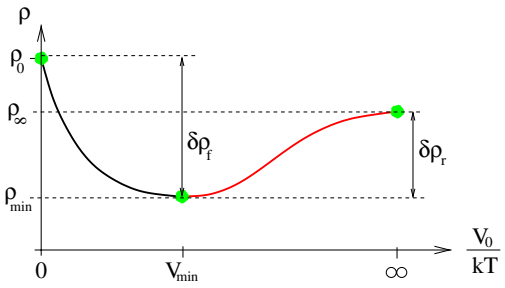

Figure 18. Schematic picture of the phase diagram.

figure 16 [41, 42], and $1/r^6$ in figure 17. There are two transition points marked at zero external potential: one calculated from $\tilde{\psi}_{G_1}$ and one from ψ_6. The reason is that there are two possible types of order: orientational order, to which ψ_6 is sensitive, and positional order, which is detected by $\tilde{\psi}_{G_1}$. The transitions for $V_0^* \neq 0$, extracted from ψ_{G_1}, for $V_0^* \to 0$ converge to the transition calculated from $\tilde{\psi}_{G_1}$. We thus define the phase boundary to be spanned by the $\tilde{\psi}_{G_1}$ transition at $V_0^* = 0$, and by the ψ_{G_1} transitions for $V_0^* \neq 0$.

Generally, beginning at zero external potential, the phase boundary bends down to lower densities for growing V_0^* and reaches a minimum at $V_0^* = 1, \ldots, 2$. Increasing V_0^* further, it turns back to higher densities and finally saturates at $V_0^* \geqslant 50$. This 'turning-back' is clearly visible in all cases except for the $1/r^6$ potential, where it seems to be less pronounced.

To quantify these observations, we define two dimensionless numbers Δ_f and Δ_r for the width of the freezing- and reentrance region:

$$\Delta_{\mathrm{f,r}} = \delta\rho_{\mathrm{f,r}}/\rho_0, \tag{35}$$

where $\delta\rho_{\mathrm{f,r}} = \rho_{0,\infty} - \rho_{\min}$; see figure 18. In the case of the DLVO potential, using $\rho = (2\kappa^2)/((\kappa a_\mathrm{s})^2\sqrt{3})$ and assuming κ as constant and a_s as variable (which is justified since only the product κa_s is important, whereas the separate values of κ and a_s are not), we can transform equation (35) into

$$\Delta_{\mathrm{f,r}} = \frac{(\kappa a_\mathrm{s})_0^2}{(\kappa a_\mathrm{s})_{0,\infty}^2} - \frac{(\kappa a_\mathrm{s})_0^2}{(\kappa a_\mathrm{s})_{\min}^2}. \tag{36}$$

Table 1. Relative density difference (equations (34), (35)) $\Delta_{f,r}$ of the freezing and reentrance region and ratio Δ_f/Δ_r for various interaction potentials, and experimental data for colloids.

	Hard disc	DLVO	$1/r^{12}$	$1/r^6$	Colloids [27]
Δ_f	0.043	0.13	0.11	0.20	0.39
Δ_r	0.028	0.028	0.029	0.016	0.10
Δ_f/Δ_r	1.5	4.6	3.8	12.5	3.9

The values of Δ_f, Δ_r and the ratio Δ_f/Δ_r for the different systems are summarized in table 1. The first four columns contain the values of our simulations, ordered from short range (left) to long range interaction (right). The last column contains the values obtained in an experiment with colloidal particles [27]. Analysing the simulations, we roughly observe an increase of the freezing region (Δ_f) when going from short to long range interactions, whereas the reentrance region (Δ_r) is nearly constant for the first three potentials. Only in the case of the $1/r^6$-potential is a drop of Δ_r found, due to the long range nature of the pair interaction.

The experimental data in the last column shows freezing- and reentrance regions which are about three times bigger than those of the corresponding DLVO simulation; the ratio Δ_f/Δ_r of the freezing- and reentrance regions, however, is nearly identical. We have also done simulations with slightly altered parameters, i.e., using particles with diameter $2R = 3\ \mu$m, effective surface charge $Z^* = 20\,000$ and $a_s = 8\ \mu$m, to match the experiments in [29] as closely as possible. Only a small shift of the phase diagram was found by $\Delta(\kappa a_s) \approx 0.35$ towards higher values of κa_s, and a negligible change in Δ_f and Δ_r. The differences between simulation and experiment may be due to the presence of many-body interactions in the experiment, which are not treated properly by the DLVO interactions used in the simulation (see [46]).

In summary, we have presented the phase diagrams of two-dimensional systems of hard [39] and various soft discs [40–42] in an external sinusoidal potential. We find an increase of the freezing region with the range of particle interaction, and a decrease of the reentrance region for the most long ranged potential $1/r^6$. The relative extent of the reentrance region is closest to the experimental data for the DLVO or the $1/r^{12}$-potentials.

6.3. Phase diagram by renormalized constants

The phase diagram of a 2D hard disc system with a modulating potential has been computed [47] as well by following a Monte Carlo renormalization approach proposed recently [48]. A cartoon of the system considered for our study is given in figure 19. For a solid in the presence of a modulating potential $\beta V(y)$ (figure 19), displacement mode u_y becomes massive, leaving massless u_x modes. After integrating out the u_y modes the free energy of the locked floating solid (LFS) may be expressed in terms of u_x and βV_0 dependent elastic moduli [32], namely, the Young's modulus K and shear modulus μ:

$$\mathcal{H}_{el} = \int \mathrm{d}x\,\mathrm{d}y \left[K \left(\frac{\partial u_x}{\partial x} \right)^2 + \mu \left(\frac{\partial u_x}{\partial y} \right)^2 \right]. \tag{37}$$

Similar arguments [32] show that among the three sets of low energy dislocations available in the 2D triangular lattice, only those (type I) with Burger's vector parallel to the line of potential minima survive at large βV_0. Dislocations with Burger's vector pointing along the other two possible close-packed directions (type II) in the 2D triangular lattice have larger energies because surrounding atoms are forced to ride the crests of the periodic potential [32]. Within this set of assumptions, the system therefore shares the same symmetries as the XY

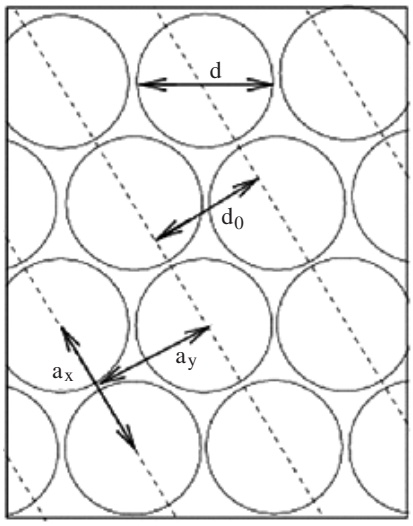

Figure 19. This cartoon shows a typical hard disc system. The dashed lines indicate minima of external modulating potential $\beta V(y) = \beta V_0 \cos(2\pi y/d_0)$. a_x is the lattice parameter and a_y indicate the average separation between two layers along the y-direction perpendicular to a set of close-packed planes. For a perfect triangular lattice $a_y = \sqrt{3}a_x/2$. The modulating potential is commensurate with the lattice such that $d_0 = a_y$, i.e., the commensurability ratio is one.

model. Indeed, a simple rescaling of $x \to \sqrt{\mu}x$ and $y \to \sqrt{K}y$ leads this free energy to the free energy of the XY model with spin-wave stiffness $K_{xy} = \sqrt{K\mu}\frac{a^2}{4\pi^2}$ and spin angle $\theta = 2\pi u_x/a_x$. The corresponding theory for phase transitions can then be recast as a KTHNY theory [17] and can be described in the framework of a two-parameter renormalization flow for the spin-wave stiffness $K(l)$ and the fugacity of type I dislocations $y'(l)$, where l is a measure of length scale as $l = \ln(r/a_x)$, r being the size of the system. The flow equations can be expressed in terms of $x' = (\pi K_{xy} - 2)$ and $y' = 4\pi \exp(-\beta E_c)$, where E_c is the core energy of type I dislocations which can be obtained from the dislocation probability [18]. Keeping up to next to leading order terms in y', the renormalization group flow equations [49, 48] are

$$\frac{dx'}{dl} = -y'^2 - y'^2 x' \tag{38}$$

$$\frac{dy'}{dl} = -x'y' + \frac{5}{4}y'^3. \tag{39}$$

Flows in l generated by the above equations starting from initial or 'bare' values of x' and y' fall in two categories. If as $l \to \infty$, $y' \to \infty$ then the thermodynamic phase is disordered (i.e., a modulated liquid (ML)), and if $y' \to 0$ it is an ordered phase (an LFS) [32]. The two kinds of flows are demarcated by the separatrix which marks the phase transition point. For the linearized equations the separatrix is simply the straight line $y' = x'$, whereas for the full non-linear equations one needs to calculate this numerically.

Again, the twin problems of diverging length and time scales are eliminated by simulating a constrained system which *does not* undergo a phase transition! This is achieved by rejecting all Monte Carlo moves which tend to distort an unit cell in a way which changes the local connectivity [18]. The percentage of moves thus rejected is a measure of the dislocation fugacity [18]. This, together with the elastic constants of the dislocation-free lattice obtained separately [50], are taken as inputs (bare values) to the renormalization flow equations [32] to find out the melting points and hence the phase diagram. The resulting phase diagram (figure 20) clearly shows a modulated liquid (ML) $\to$ locked floating solid (LFS) $\to$ ML reentrant transition with increase in the amplitude (V_0) of the potential. In general, the predictions of the theory of [32] appear to be valid. The locations of the phase transitions as evaluated within this theory with our inputs, however, do *not* agree with earlier simulations [39]

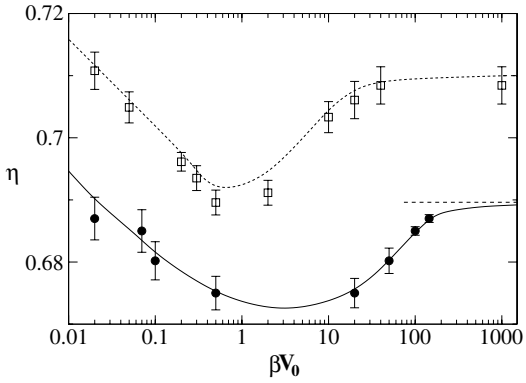

Figure 20. The phase diagram of the hard disc system in the presence of a 1D, commensurate, periodic potential in the packing fraction ($\eta = (\pi/4)\rho d^2$)-potential strength (βV_0) plane. The lines in the figure are a guide to the eye. The dashed curve denotes earlier Monte Carlo simulation results [39] and the solid curve is calculated through the numerical renormalization group study [47]. The dotted curve at $\eta \simeq 0.69$ denotes the calculated asymptotic phase transition point at $\beta V_0 = \infty$.

throughout the η–βV_0 plane. The phase diagram here is obtained by solving the flow equations correct to third order in the defect fugacity; inclusions of still higher order terms may improve the agreements with simulations.

Acknowledgments

We thank the NIC and the HLRS for computer time. This work was supported by the SFB TR6, the SFB 513 and the DFG-IRTG 'Soft Condensed Matter'. SS acknowledges The Humboldt Foundation and Department of Science and Technology, Government of India grant no. SP/S2/M-20/2001 and DC acknowledges CSIR, India for support.

References

[1] Landau D P and Binder K 2000 *A Guide to Monte Carlo Simulations in Statistical Physics* (Cambridge: Cambridge University Press)
[2] Nielaba P, Mareschal M and Ciccotti G (ed) 2002 *Bridging Time Scales: Molecular Simulations for the Next Decade* (Berlin: Springer)
[3] Sengupta S, Nielaba P, Rao M and Binder K 2000 *Phys. Rev.* E **61** 1072
[4] Chaikin P M and Lubensky T C 1995 *Principles of Condensed Matter Physics* (Cambridge: Cambridge University Press)
[5] Wallace D C 1958 *Solid State Physics* ed H Ehrenreich, F Seitz and D Turnbull (New York: Academic)
Weiner J H 1983 *Statistical Mechanics of Elasticity* (New York: Wiley)
[6] Wojciechowski K W and Brańka A C 1988 *Phys. Lett.* A **134** 314
[7] Seitz F 1940 *Modern Theory of Solids* (New York: McGraw-Hill)
Born M and Huang K 1954 *Dynamical Theory of Crystal Lattices* (Oxford: Oxford University Press)
For experimental temperature dependent elastic constants of solid argon see: Meixner H, Leiderer P, Berberich P and Lüscher E 1972 *Phys. Lett.* A **40** 257
[8] Ryzhov V N and Tareyeva E E 1995 *Phys. Rev.* B **51** 8789
[9] Zahn K, Wille A, Maret G, Sengupta S and Nielaba P 2003 *Phys. Rev. Lett.* **90** 155506
[10] Franzrahe K 2004 *PhD Thesis* in work
[11] Henseler P 2004 *PhD Thesis* in work
[12] Alder B J and Wainwright T E 1962 *Phys. Rev.* **127** 359
[13] Lee J and Strandburg K 1992 *Phys. Rev.* B **46** 11190

[14] Zollweg J A and Chester G V 1992 *Phys. Rev.* B **46** 11186
[15] Ramakrishnan T V 1979 *Phys. Rev. Lett.* **42** 795
Zeng X C and Oxtoby D W 1990 *J. Chem. Phys.* **93** 2692
Rosenfeld Y 1990 *Phys. Rev.* A **42** 5978
[16] Jaster A 1999 *Phys. Rev.* E **59** 2594
Jaster A 2000 *Physica* A **277** 106
[17] Kosterlitz J M and Thouless D J 1973 *J. Phys. C: Solid State Phys.* **6** 1181
Halperin B I and Nelson D R 1978 *Phys. Rev. Lett.* **41** 121
Nelson D R and Halperin B I 1979 *Phys. Rev.* B **19** 2457
Young A P 1979 *Phys. Rev.* B **19** 1855
[18] Sengupta S, Nielaba P and Binder K 2000 *Phys. Rev.* E **61** 6294
[19] Zahn K, Lenke R and Maret G 1999 *Phys. Rev. Lett.* **82** 2721
[20] Bates M and Frenkel D 2000 *Phys. Rev.* E **61** 5223
[21] Binder K, Sengupta S and Nielaba P 2002 *J. Phys.: Condens. Matter* **14** 2323
[22] Ricci A 2004 *PhD Thesis* in work
[23] Broughton J Q, Gilmer G H and Weeks J D 1982 *Phys. Rev.* B **25** 4651
[24] Clark N A, Ackerson B J and Hurd A J 1983 *Phys. Rev. Lett.* **50** 1459
[25] Chowdhury A, Ackerson B J and Clark N A 1985 *Phys. Rev. Lett.* **55** 833
[26] Loudiyi K and Ackerson B J 1992 *Physica* A **184** 1
Loudiyi K and Ackerson B J 1992 *Physica* A **184** 26
[27] Wei Q-H, Bechinger C, Rudhardt D and Leiderer P 1998 *Phys. Rev. Lett.* **81** 2606
[28] Bechinger C, Wei Q H and Leiderer P 2000 *J. Phys.: Condens. Matter* **12** A425
[29] Bechinger C, Brunner M and Leiderer P 2001 *Phys. Rev. Lett.* **86** 930
[30] Chakrabarti J, Krishnamurthy H R and Sood A K 1994 *Phys. Rev. Lett.* **73** 2923
[31] Rasmussen L L and Oxtoby D W 2002 *J. Phys.: Condens. Matter* **14** 12021
[32] Frey E, Nelson D R and Radzihovsky L 1999 *Phys. Rev. Lett.* **83** 2977
Radzihovsky L, Frey E and Nelson D R 2001 *Phys. Rev.* E **63** 031503
[33] Chakrabarti J, Krishnamurthy H R, Sood A K and Sengupta S 1995 *Phys. Rev. Lett.* **75** 2232
[34] Das C and Krishnamurthy H R 1998 *Phys. Rev.* B **58** R5889
[35] Das C, Sood A K and Krishnamurthy H R 1999 *Physica* A **270** 237
[36] Das C, Chaudhuri P, Sood A and Krishnamurthy H 2001 *Curr. Sci.* **80** 959
[37] For an introduction to phase transitions in colloids see, Sood A K 1991 *Solid State Physics* vol 45, ed E Ehrenfest and D Turnbull (New York: Academic) p 1
Pusey P N 1991 *Liquids, Freezing and the Glass Transition* ed J P Hansen and J Zinn-Justin (Amsterdam: North-Holland)
[38] Strepp W, Lohrer M, Sengupta S and Nielaba P 2004 *Preprint*
[39] Strepp W, Sengupta S and Nielaba P 2001 *Phys. Rev.* E **63** 046106
[40] Strepp W, Sengupta S and Nielaba P 2002 *Phys. Rev.* E **66** 056109
[41] Strepp W, Sengupta S, Lohrer M and Nielaba P 2002 *Comput. Phys. Commun.* **147** 370–3
[42] Strepp W, Sengupta S, Lohrer M and Nielaba P 2003 *Math. Comput. Simul.* **62** 519
[43] Binder K 1981 *Z. Phys.* B **43** 119
Binder K 1981 *Phys. Rev. Lett.* **47** 693
[44] Vollmayr K, Reger J D, Scheucher M and Binder K 1993 *Z. Phys.* B **91** 113
[45] Metropolis N, Rosenbluth A W, Rosenbluth M N, Teller A H and Teller E 1953 *J. Chem. Phys.* **21** 1087
[46] Brunner M, Bechinger C, Strepp W, Lobaskin V and von Gruenberg H H 2002 *Europhys. Lett.* **58** 926
[47] Chaudhuri D and Sengupta S 2004 *Preprint* cond-mat/0403319
[48] Sengupta S, Nielaba P and Binder K 2000 *Europhys. Lett.* **50** 668
[49] Amit D J *et al* 1980 *J. Phys. A: Math. Gen.* **13** 585
[50] Farago O and Kantor Y 2000 *Phys. Rev.* E **61** 2478